Real-Time Dynamic Modeling – Data Information Requirements and Flight Test Results

Eugene A. Morelli [1]
NASA Langley Research Center, Hampton, Virginia, 23681

Mark S. Smith [2]
NASA Dryden Flight Research Center, Edwards, California, 93523

Practical aspects of identifying dynamic models for aircraft in real time were studied. Topics include formulation of an equation-error method in the frequency domain to estimate non-dimensional stability and control derivatives in real time, data information content for accurate modeling results, and data information management techniques such as data forgetting, incorporating prior information, and optimized excitation. Real-time dynamic modeling was applied to simulation data and flight test data from a modified F-15B fighter aircraft, and to operational flight data from a subscale jet transport aircraft. Estimated parameter standard errors, prediction cases, and comparisons with results from a batch output-error method in the time domain were used to demonstrate the accuracy of the identified real-time models.

Nomenclature

a_x, a_y, a_z	=	body-axis translational accelerometer measurements, g or ft/sec^2
b	=	wing span, ft
$\bar{c}$	=	mean aerodynamic chord, ft
C_X, C_Y, C_Z	=	body-axis non-dimensional aerodynamic force coefficients
C_l, C_m, C_n	=	body-axis non-dimensional aerodynamic moment coefficients
$E\{\ \}$	=	expectation operator
I_x, I_y, I_z, I_{xz}	=	mass moments of inertia, slug-ft^2
j	=	imaginary number = $\sqrt{-1}$
J	=	cost function
m	=	aircraft mass, slug
M_T	=	body-axis pitching moment from engine thrust, ft-lbf
p, q, r	=	body-axis roll, pitch, and yaw rates, rad/sec or deg/sec
$\bar{q}$	=	dynamic pressure, lbf/ft^2
s	=	standard error
S	=	wing reference area, ft^2
T	=	maneuver length, sec
T_x, T_z	=	body-axis engine thrust, lbf
V	=	airspeed, ft/sec
α	=	angle of attack, rad or deg
β	=	sideslip angle, rad or deg
$\delta_e, \delta_a, \delta_r, \delta_f$	=	elevator, aileron, rudder, and trailing-edge flap deflections, rad or deg
$\delta_c, \delta_{dc}, \delta_s, \delta_{ds}$	=	canard, differential canard, stabilator, and differential stabilator deflections, rad or deg

[1] Research Engineer, Dynamic Systems and Control Branch, MS 308, Associate Fellow
[2] Research Engineer, Aerodynamics Branch, P.O. Box 273

φ, θ, ψ	=	Euler roll, pitch, and yaw angles, rad or deg
θ	=	parameter vector
Σ	=	covariance matrix
ω	=	frequency, rad/sec

superscripts

T	=	transpose
$\dagger$	=	complex conjugate transpose
$\hat{}$	=	estimate
$\dot{}$	=	time derivative
$\tilde{}$	=	Fourier transform
-1	=	matrix inverse

subscripts

o	=	reference value

I. Introduction

DYNAMIC modeling in real time has many important practical uses, such as improving the efficiency of stability and control flight testing, flight envelope expansion, adaptive or reconfigurable control, vehicle health monitoring, and fault detection. Several methods[1-5] have been investigated for identifying local linear dynamic models from flight data in real time. One of these methods[4,6] is based on a recursive Fourier transform and equation-error modeling in the frequency domain. This method, sometimes called the Fourier Transform Regression (FTR) method, produces very accurate results with valid error measures and has many practical advantages. The FTR method has also been independently evaluated[7,8] as the best method available for real-time dynamic modeling. For these reasons, the FTR method was chosen for further study and application.

The FTR method has been successfully applied[4,6-11] to identify accurate linear dynamic models in real time at individual flight conditions. While this capability is important and useful, further progress requires that this capability be extended to continuous application as the aircraft flies through a wide range of changing flight conditions throughout the flight envelope. Ultimately, local real-time modeling results could be integrated into a global aerodynamic model that could be updated in real time as the aircraft changes flight conditions, changes configuration, ages, or becomes damaged in some way. This vision of real-time global dynamic modeling has many important implications for efficient flight testing, accurate flight simulation, adaptive or reconfigurable control, and aircraft safety.

One important aspect of applying real-time dynamic modeling for varying flight conditions and aircraft configurations is determining the data information content requirements for accurate dynamic modeling results. Changing aircraft flight conditions or aircraft configurations means that parameters in the approximating dynamic model change. Dynamic motion of the aircraft, either from ordinary flight operations or from applied control surface excitation, is necessary so that the measured data will exhibit the aircraft dynamics to be modeled. Naturally, if the real-time dynamic modeling is to be done continuously or on a regular basis, it is important that only the minimum necessary aircraft excitation be applied, and the resulting aircraft motion should be as small and unobtrusive as possible.

This paper investigates data information requirements for accurate real-time dynamic modeling. Flight experiments on a modified F-15B fighter aircraft are used to illuminate issues related to data information content necessary for accurate real-time modeling. Real-time modeling is also applied to operational flight data from a subscale jet transport model, to evaluate the feasibility of real-time modeling without specific excitation. This is an important step in extending local real-time modeling to the case of changing conditions, interpreted broadly to include flight condition changes, configuration changes, damage, and failure scenarios. Issues such as data information content necessary for fast and accurate local modeling, model validation, necessary excitation, data forgetting, and methods for incorporating prior information are studied.

The next section describes the methods used. A model formulation is developed that retains full nonlinear dynamics, with linearized aerodynamic models. The FTR method is described, along with explanations of methods for data forgetting and incorporating prior information into the real-time parameter estimation algorithm. Next, the flight test aircraft are described, including flight instrumentation and characteristics of the flight data. The results section includes simulation and flight test investigations examining data information requirements for accurately

identifying local dynamic models in real time. Finally, the concluding remarks summarize progress made so far and outline some possible next steps.

II. Methods

A. Aerodynamic Modeling

Non-dimensional aerodynamic force and moment coefficients for an aircraft can be computed from flight measurements as follows[6]:

$$C_X = \frac{1}{\bar{q}S}\left(m a_x - T_x\right) \tag{1a}$$

$$C_Z = \frac{1}{\bar{q}S}\left(m a_z - T_z\right) \tag{1b}$$

$$C_m = \frac{1}{\bar{q}S\bar{c}}\left[I_y \dot{q} + \left(I_x - I_z\right) pr + I_{xz}\left(p^2 - r^2\right) - M_T \right] \tag{1c}$$

$$C_Y = \frac{m a_y}{\bar{q}S} \tag{2a}$$

$$C_l = \frac{1}{\bar{q}Sb}\left[I_x \dot{p} - I_{xz}\left(pq + \dot{r}\right) + \left(I_z - I_y\right) qr \right] \tag{2b}$$

$$C_n = \frac{1}{\bar{q}Sb}\left[I_z \dot{r} - I_{xz}\left(\dot{p} - qr\right) + \left(I_y - I_x\right) pq \right] \tag{2c}$$

These expressions retain the full nonlinear dynamics in the aircraft equations of motion. For local real-time modeling over a short time period, the force and moment coefficients computed from Eqs. (1) and (2) can be modeled using linear expansions in the aircraft states and controls:

$$C_X = C_{X_\alpha}\Delta\alpha + C_{X_q}\frac{\Delta q\bar{c}}{2V} + C_{X_\delta}\Delta\delta + C_{X_o} \tag{3a}$$

$$C_Z = C_{Z_\alpha}\Delta\alpha + C_{Z_q}\frac{\Delta q\bar{c}}{2V} + C_{Z_\delta}\Delta\delta + C_{Z_o} \tag{3b}$$

$$C_m = C_{m_\alpha}\Delta\alpha + C_{m_q}\frac{\Delta q\bar{c}}{2V} + C_{m_\delta}\Delta\delta + C_{m_o} \tag{3c}$$

$$C_Y = C_{Y_\beta}\Delta\beta + C_{Y_p}\frac{\Delta pb}{2V} + C_{Y_r}\frac{\Delta rb}{2V} + C_{Y_\delta}\Delta\delta + C_{Y_o} \tag{4a}$$

$$C_l = C_{l_\beta}\Delta\beta + C_{l_p}\frac{\Delta pb}{2V} + C_{l_r}\frac{\Delta rb}{2V} + C_{l_\delta}\Delta\delta + C_{l_o} \tag{4b}$$

$$C_n = C_{n_\beta}\Delta\beta + C_{n_p}\frac{\Delta pb}{2V} + C_{n_r}\frac{\Delta rb}{2V} + C_{n_\delta}\Delta\delta + C_{n_o} \tag{4c}$$

The Δ notation indicates perturbation from a reference condition. In each expansion, a single term is shown to represent all relevant and similar control terms, to simplify the expressions. For example, in Eq. (3c), the term

$C_{m_\delta}\Delta\delta$ represents all the control terms for C_m, e.g., $C_{m_\delta}\Delta\delta \equiv C_{m_{\delta_e}}\Delta\delta_e + C_{m_{\delta_f}}\Delta\delta_f$. In Eq. (3c), C_{m_o} represents the non-dimensional pitching moment at a reference condition, and similarly for the other expansions.

The linear aerodynamic models in Eqs. (3) and (4) contain parameters called stability and control derivatives, such as C_{m_α} and C_{m_δ}, which characterize the stability and control of the aircraft. For short periods of time, the stability and control derivatives are considered to be constant model parameters to be estimated from flight data. Repeating the parameter estimation at short time intervals produces piecewise constant estimates for the stability and control derivatives, which in general vary with flight condition and changes to the aircraft, such as configuration, age, damage, or failures.

The next subsection describes how the unknown stability and control derivatives in the linear aerodynamic models of Eqs. (3) and (4) can be estimated from flight data using equation-error parameter estimation in the frequency domain.

B. Stability and Control Derivative Estimation in the Frequency Domain

This section describes the FTR method for estimating unknown parameters in a dynamic model in real time. Some of the material presented here can also be found in Refs. 4 and 6.

The first step required for modeling in the frequency domain is to transform the measured flight data from the time domain into the frequency domain. The finite Fourier transform is the analytical tool used for this task. For an arbitrary scalar signal $x(t)$ on the time interval $[0,T]$, the finite Fourier transform is defined by

$$\mathcal{F}\left[x(t)\right] \equiv \tilde{x}(\omega) \equiv \int_0^T x(t)\, e^{-j\omega t} dt \tag{5}$$

which can be approximated by

$$\tilde{x}(\omega) \approx \Delta t \sum_{i=0}^{N-1} x(i)\, e^{-j\omega i \Delta t} \tag{6}$$

where $x(i) \equiv x(i\Delta t)$, $T = N\Delta t$, and Δt is a constant sampling interval. The summation in Eq. (6) is defined as the discrete Fourier transform,

$$X(\omega) \equiv \sum_{i=0}^{N-1} x(i)\; e^{-j\omega i \Delta t} \tag{7}$$

so that the finite Fourier transform approximation in Eq. (6) can be written as

$$\tilde{x}(\omega) \approx X(\omega)\; \Delta t \tag{8}$$

Some fairly straightforward corrections[12] can be made to remove the inaccuracy resulting from the fact that Eq. (8) is a simple Euler approximation to the finite Fourier transform of Eq. (5). However, if the sampling rate is much higher than the frequencies of interest, as is typically the case for dynamic modeling from flight data, then the corrections are small and can be safely ignored.

The Fourier transform is applied to the non-dimensional force and moment coefficients computed from Eqs. (1) and (2) using measured time-domain data. This results in the non-dimensional force and moment coefficients in the frequency domain. Often, measurements of the angular accelerations $\dot{p}, \dot{q}, \text{and } \dot{r}$ are not available. In the frequency domain, these derivatives can be calculated by multiplying the Fourier transforms of $p, q, \text{and } r$ by $j\omega$. For example, the Fourier transform of the rolling moment coefficient can be computed as:

$$\tilde{C}_l(\omega) \equiv \mathcal{F}\left[C_l\right] = \; j\omega\,\mathcal{F}\left[\frac{I_x p - I_{xz} r}{\bar{q}Sb}\right] + \mathcal{F}\left[\frac{-I_{xz} pq + \left(I_z - I_y\right) qr}{\bar{q}Sb}\right] \tag{9}$$

and similarly for C_m and C_n. This approach implements the derivative of the body-axis angular momentum in the frequency domain, including the time variation in the inertia quantities. Note that the Fourier transform of the nonlinear terms is handled by computing the nonlinear terms in the time domain, then applying the Fourier transform to the resulting time history. Treatment of the dynamic pressure $\bar{q}$ in Eq. (9) is consistent with an assumption that the dynamic pressure varies slowly, which is a good practical assumption.

To obtain the perturbation states and controls in Eqs. (3) and (4), time histories of the measured states and controls are high-pass filtered to remove the steady part of each signal. Then, each perturbation signal is transformed into the frequency domain using the discrete Fourier transform. The break frequency for the high-pass filter is set just below the lowest frequency selected for the modeling. High-pass filtering is implemented with a fourth-order Butterworth digital filter. Similarly, the quantities transformed in Eq. (9) (shown within the square brackets) are high-pass filtered prior to Fourier transformation. This approach effectively drops out the bias terms in the models of Eqs. (3) and (4). The high-pass filtering also prevents leakage from the relatively large spectral component at zero frequency, associated with the steady component of each signal, from polluting transformed data at low frequencies.

For each aerodynamic model in Eqs. (3) and (4), the parameter estimation problem can be formulated as a standard least squares regression problem with complex data[6],

$$\tilde{\boldsymbol{z}} = \tilde{\boldsymbol{X}}\boldsymbol{\theta} + \tilde{\boldsymbol{e}} \tag{10}$$

where, for example, using the pitching moment equation (3c),

$$\tilde{\boldsymbol{z}} = \begin{bmatrix} \tilde{C}_m(1) \\ \tilde{C}_m(2) \\ \vdots \\ \tilde{C}_m(M) \end{bmatrix} \tag{11}$$

$$\tilde{\boldsymbol{X}} = \begin{bmatrix} \Delta\tilde{\alpha}(1) & \Delta\tilde{q}_n(1) & \Delta\tilde{\delta}_e(1) & \Delta\tilde{\delta}_f(1) \\ \Delta\tilde{\alpha}(2) & \Delta\tilde{q}_n(2) & \Delta\tilde{\delta}_e(2) & \Delta\tilde{\delta}_f(2) \\ \vdots & \vdots & \vdots & \vdots \\ \Delta\tilde{\alpha}(M) & \Delta\tilde{q}_n(M) & \Delta\tilde{\delta}_e(M) & \Delta\tilde{\delta}_f(M) \end{bmatrix} \tag{12}$$

$$\boldsymbol{\theta} = \begin{bmatrix} C_{m_\alpha} \\ C_{m_q} \\ C_{m_{\delta_e}} \\ C_{m_{\delta_f}} \end{bmatrix} \tag{13}$$

The notation $\Delta\tilde{q}_n$ represents $\mathcal{F}\left[q\bar{c}/(2V)\right]$ and $\tilde{\boldsymbol{e}}$ represents the complex equation error vector in the frequency domain. The symbols $\Delta\tilde{\alpha}(k)$, $k = 1, 2, \ldots, M$ denote the Fourier transform of the angle of attack perturbation state for each frequency ω_k, and similarly for other quantities. Each transformed variable depends on frequency. The

frequencies ω_k can be chosen arbitrarily, and are therefore chosen to cover the frequency band where the aircraft dynamics lie, as will be discussed later. The least squares cost function is

$$J(\theta) = \frac{1}{2}\left(\tilde{\boldsymbol{z}} - \tilde{\boldsymbol{X}}\,\theta\right)^{\dagger}\left(\tilde{\boldsymbol{z}} - \tilde{\boldsymbol{X}}\,\theta\right) \tag{14}$$

This cost function contains *M* squared error terms in summation, corresponding to *M* frequencies of interest. Similar cost expressions can be written for individual lines from Eqs. (3) and (4). The parameter vector estimate that minimizes the least squares cost function is computed from[6]

$$\hat{\theta} = \left[Re\left(\tilde{\boldsymbol{X}}^{\dagger}\,\tilde{\boldsymbol{X}}\right)\right]^{-1} Re\left(\tilde{\boldsymbol{X}}^{\dagger}\,\tilde{\boldsymbol{z}}\right) \tag{15}$$

The estimated parameter covariance matrix is[6]

$$Cov\left(\hat{\theta}\right) \equiv E\left\{\left(\hat{\theta}-\theta\right)\left(\hat{\theta}-\theta\right)^{T}\right\} = \sigma^2\left[Re\left(\tilde{\boldsymbol{X}}^{\dagger}\,\tilde{\boldsymbol{X}}\right)\right]^{-1} \tag{16}$$

where the equation-error variance σ^2 can be estimated from the residuals,

$$\hat{\sigma}^2 = \frac{1}{\left(M - n_p\right)}\left[\left(\tilde{\boldsymbol{z}} - \tilde{\boldsymbol{X}}\,\hat{\theta}\right)^{\dagger}\left(\tilde{\boldsymbol{z}} - \tilde{\boldsymbol{X}}\,\hat{\theta}\right)\right] \tag{17}$$

and n_p is the number of unknown parameters, i.e., the number of elements in parameter vector θ. Parameter standard errors are computed as the square root of the diagonal elements of the $Cov\left(\hat{\theta}\right)$ matrix from Eq. (16), using $\hat{\sigma}^2$ from Eq. (17). Reference 6 explains why the estimated parameter standard errors are computed in this way, and also why this calculation in the frequency domain produces parameter error measures that are consistent with the scatter in parameter estimates from repeated maneuvers. Realistic simulation testing has shown that the accuracy of model parameters estimated with this method is comparable to using a time-domain output-error method employing iterative nonlinear optimization in post-flight batch mode[13].

The model formulation given here is widely applicable, because the assumption of constant linear aerodynamic models over short time periods is very accurate for non-dimensional stability and control derivatives, where the effects of changing dynamic pressure and mass properties are removed.

To implement this least squares parameter estimation in the frequency domain, the parameter estimation calculations in Eqs. (15)-(17) are applied to frequency-domain data at selected times, normally at regular time intervals. The frequency-domain data must therefore be available at any time, so the Fourier transforms are computed using a recursive Fourier transform, described next.

C. Recursive Fourier Transform

For a given frequency ω, the discrete Fourier transform in Eq. (7) at time $i\,\Delta t$, denoted by $X_i(\omega)$, is related to the discrete Fourier transform at time $(i-1)\,\Delta t$ by

$$X_i(\omega) = X_{i-1}(\omega) + x(i)\,e^{-j\omega i\Delta t} \tag{18}$$

where

$$e^{-j\omega i\Delta t} = e^{-j\omega\Delta t}\;e^{-j\omega(i-1)\Delta t} \tag{19}$$

The quantity $e^{-j\omega\Delta t}$ is constant for a given frequency ω and constant sampling interval Δt. It follows that the discrete Fourier transform can be computed for a given frequency at each time step using one addition in Eq. (18) and two multiplications – one in Eq. (19) using the stored constant $e^{-j\omega\Delta t}$ for frequency ω, and one in Eq. (18). There is no need to store the time-domain data in memory when computing the discrete Fourier transform in this way, because the data for each sample time is processed immediately. Time-domain data from the past can be used in all subsequent analysis by simply continuing the recursive calculation of the Fourier transform. In this sense, the recursive Fourier transform acts as memory for the information in the data. More data from more maneuvers improves the quality of the data in the frequency domain without increasing memory requirements to store it. Furthermore, the Fourier transform is available at any time $i\,\Delta t$. The approximation to the finite Fourier transform is completed using Eq. (8).

The recursive computation of the Fourier transform does not use a Fast Fourier Transform (FFT) algorithm[14], and therefore would be comparatively slow, if the entire frequency band up to the Nyquist frequency $1/(2\Delta t)$ were of interest. However, rigid-body dynamics of aircraft lie in a rather narrow frequency band of approximately 0.01-2.0 Hz. Since the frequency band is limited, it is efficient to compute the discrete Fourier transform using Eqs. (18) and (19) (which represents a recursive formulation of Eq. (7)) for only the selected frequencies ω_k, $k = 1,2,\ldots,M$. With this approach, it is possible to select closely-spaced fixed frequencies for the Fourier transform and the subsequent modeling and still do the calculations efficiently.

Using a limited frequency band for the Fourier transformation confines the data analysis to the frequency band where the dynamics lie, and automatically filters wide band measurement noise or structural responses outside the frequency band of interest. These automatic filtering features are important for real-time applications, where instrumentation error corrections and noise filtering would require additional computational resources.

In past work on fighter aircraft short-period modeling, frequency spacing of 0.04 Hz on an interval of approximately [0.1-2] Hz was found to be adequate[9-11]. Finer frequency spacing requires slightly more computation, but was found to have little effect on the results. When the frequency spacing is very coarse, there is a danger of omitting important frequency components, and this can lead to inaccurate parameter estimates. In general, a good rule of thumb is to use frequencies evenly spaced at 0.04 Hz over the bandwidth for the dynamic system. For good results, the bandwidth should be limited to the frequency range where the signal components in the frequency domain are at least twice the amplitude of the wide band noise level. However, the algorithm is robust to these design choices, so the selections to be made are not difficult.

The recursive Fourier transform update need not be done for every sampled time point. Systematically skipping time points effectively lowers the sampling rate of the data prior to Fourier transformation. This saves computation, and does not have a significant adverse impact on the parameter estimation results until the Fourier transform update rate gets below approximately 5 times the highest frequency of interest for the dynamic system. The parameter estimation and covariance calculations in Eqs. (15)-(17) can be done at any time, but are usually done at 1 or 2 Hz, to save computations. Linearized aerodynamic characteristics rarely change faster than this, except in cases of strong nonlinearity, damage, failure, or rapid maneuvering. For these cases, the update rate can be increased, at the cost of more computations.

Reference 6 explains that computing standard errors from the covariance matrix in Eq. (16) does not require correction for colored residuals. The standard errors computed from Eq. (16) are therefore a good representation of the error in the estimated parameters. Having high quality error measures is important for problems such as failure detection and control law reconfiguration.

D. Data Forgetting

The recursive Fourier transform in Eqs. (18) and (19) represents a data information memory for as long as the running sum is incremented. It follows that when the aircraft dynamics change, the older data should be discounted in some way, as has been done for time-domain approaches using a forgetting factor[6]. If this is not done, then the speed of response for the real-time parameter estimator is progressively degraded, as new information has to overwhelm an increasingly longer memory. Consequently, there is a trade-off between the desired rapid response of the parameter estimator to changes in the aircraft dynamics, versus retaining enough information from past data for sufficiently accurate model parameter estimates.

If past values of the Fourier transform $X_i(\omega)$ computed from Eq. (18) are saved in computer memory, then it is possible to implement selective amnesia by simply subtracting past values of the running sum corresponding to the

Fourier transform, or differences between past values of the running sum. For example, forgetting all data information content older than 10 sec (i.e., removing that data information content from the complex regression problem) could be implemented by subtracting the value of the running sums for the Fourier transforms at 10 sec ago from the current running sums. Similarly, to forget data information content collected between 5 and 7 sec ago, the difference between the running sums at 5 and 7 sec ago would be subtracted from the current running sum. The price to pay for this capability is the computer memory required to store past values of the running sums associated with the Fourier transforms for each signal at each frequency. The memory requirements could be reduced by perhaps only saving the running sums at intervals of 0.5 sec, for example.

The simplicity of Eq. (18) also makes it easy to see how exponential data forgetting could be implemented. In exponential data forgetting, each past value of the time-domain signal is multiplied by a forgetting factor $\lambda < 1$ at each time step. In this way, old data is gradually devalued and eventually discarded. Usually, λ is chosen in the range $0.90 \le \lambda < 1.00$. To implement this, Eq. (18) is modified slightly to

$$X_i(\omega) = \lambda X_{i-1}(\omega) + x(i)\, e^{-j\omega i \Delta t} \tag{20}$$

and everything else remains the same as before. This simple approach is possible because the Fourier transform is linear with respect to the measured data $x(i)$.

The challenge with data forgetting is not in the implementation, but rather in deciding how much data information content to forget, and when. At the present time, there are no concrete guidelines, so the choices are made based on analysis of results from simulation and flight data.

E. Incorporating Prior Information

Model parameter estimates can sometimes be improved by including information based on models identified from prior data. In the case of real-time dynamic modeling, including prior information of this kind can reduce variations in the real-time parameter estimates, and improve convergence speed.

One way to incorporate prior information is by using a mixed estimator formulation of the least squares cost function[6]. Assuming that the fit error variance σ_p^2 for the prior modeling is approximately equal to the fit error variance σ^2 for a model based on the current data alone, and denoting the vector of parameter estimates from a prior analysis by $\boldsymbol{\theta}_p$, with associated covariance matrix $\boldsymbol{\Sigma}_p$, the least squares cost function that incorporates this prior information is formulated as[6]

$$J(\boldsymbol{\theta}) = \frac{1}{2}\left(\tilde{\boldsymbol{z}} - \tilde{\boldsymbol{X}}\boldsymbol{\theta}\right)^{\dagger}\left(\tilde{\boldsymbol{z}} - \tilde{\boldsymbol{X}}\boldsymbol{\theta}\right) + \frac{1}{2}\left(\boldsymbol{\theta} - \boldsymbol{\theta}_p\right)^{T}\boldsymbol{\Sigma}_p^{-1}\left(\boldsymbol{\theta} - \boldsymbol{\theta}_p\right) \tag{21}$$

The vector of parameter estimates that minimize this modified least squares cost function is

$$\hat{\boldsymbol{\theta}} = \left[Re\left(\tilde{\boldsymbol{X}}^{\dagger}\tilde{\boldsymbol{X}}\right) + \boldsymbol{\Sigma}_p^{-1}\right]^{-1}\left[Re\left(\tilde{\boldsymbol{X}}^{\dagger}\tilde{\boldsymbol{z}}\right) + \boldsymbol{\Sigma}_p^{-1}\boldsymbol{\theta}_p\right] \tag{22}$$

with covariance matrix

$$Cov\left(\hat{\boldsymbol{\theta}}\right) = \sigma^2\left[Re\left(\tilde{\boldsymbol{X}}^{\dagger}\tilde{\boldsymbol{X}}\right) + \boldsymbol{\Sigma}_p^{-1}\right]^{-1} \tag{23}$$

where σ^2 is estimated from Eq. (17), as before. Reference 6 provides further details on the mixed estimator formulation of the least squares parameter estimation problem, and the associated solution.

F. Optimized Excitation

References 6, 11, and 15 describe a method for designing optimized inputs for use as control surface perturbations to excite aircraft dynamics. The form of each input is a sum of sinusoids with unique frequencies and

phase shifts. Multiple inputs are designed to be mutually orthogonal in both the time domain and the frequency domain, and are optimized for maximum data information content in multiple axes over a short time period, while minimizing excursions from the nominal flight condition. The mutual orthogonality of the inputs allows simultaneous application of multiple inputs, which helps to minimize excitation time. Optimized inputs of this type were applied to the modified F-15B to collect data for real-time dynamic modeling. The optimized inputs were applied as control surface excitations by summation with the actuator commands from the control system just before the actuator command rate and position limiting. Flight test examples are shown below in the Results section.

III. Test Aircraft and Flight Data

A. Fighter Aircraft Description

The fighter aircraft used for this research is a pre-production Boeing F-15B that has been highly modified to support various test programs. The most visible modification is the inclusion of a set of canards near the pilot station, see Fig. 1. The canards are a set of modified horizontal stabilators from a Boeing F/A-18 aircraft. The purpose of the canard addition was to increase maneuverability and load capability. An additional effect of the canards was to cause the aircraft to be statically unstable longitudinally at most subsonic speeds. The propulsion system consists of two Pratt & Whitney F100-PW-229 engines, each equipped with an axisymmetric thrust vectoring pitch/yaw balance beam nozzle. The thrust vectoring feature, however, was not used during the flight testing described here. Further information on the modified F-15B aircraft and associated flight test operations can be found in Ref. 16.

Figure 1. **Modified F-15B Fighter Jet Aircraft**

1. Control Surfaces

The aircraft has five pairs of control surfaces: stabilators, canards, ailerons, trailing edge flaps, and rudders. Flaps and aileron droop are manually set by the pilot and only used for takeoff and landing configurations. Conventional pitch control is provided by symmetric deflection of the all-moving horizontal stabilators and canards. Roll control uses aileron and differential stabilator. Directional control is provided by rudder and differential canard deflection. Definitions of control surface deflections are given below. Trailing edge down is positive deflection for the wing and stabilator surfaces, and trailing edge left is positive for the rudder.

$$\delta_s = \frac{1}{2}\left(\delta_{s_{right}} + \delta_{s_{left}}\right) \qquad \delta_c = \frac{1}{2}\left(\delta_{c_{right}} + \delta_{c_{left}}\right) \tag{24a}$$

$$\delta_a = \frac{1}{2}\left(\delta_{a_{right}} - \delta_{a_{left}}\right) \qquad \delta_r = \frac{1}{2}\left(\delta_{r_{right}} + \delta_{r_{left}}\right) \qquad \delta_{dc} = \frac{1}{2}\left(\delta_{c_{right}} - \delta_{c_{left}}\right) \qquad \delta_{ds} = \frac{1}{2}\left(\delta_{s_{right}} - \delta_{s_{left}}\right) \tag{24b}$$

For the nominal flight control system, pilot stick and rudder pedal inputs result in high correlation between the symmetric canard and angle of attack, rudder and differential canard, and differential stabilator and aileron. Flight data analysis showed that the symmetric canard and angle of attack exhibited nominal pair-wise correlation of 0.93, rudder and differential canard were correlated at 0.99, and the differential stabilator and aileron were perfectly correlated at 1.00. Given these high levels of correlated inputs, it would be impossible with pilot input maneuvers to distinguish, for example, between rolling moment generated by the aileron and rolling moment generated by the differential stabilator. Consequently, the complete stability and control derivative set cannot be obtained with pilot input maneuvers.

2. Instrumentation and Data Acquisition

The modified F-15B aircraft was equipped with a research-quality instrumentation system. A nose boom was installed and calibrated for free stream pitot-static pressure and flow angle measurements. An inertial instrumentation package provided 3-axis linear accelerometer and angular rate measurements. Heading, pitch, and bank angle were obtained from the aircraft inertial navigation system. Control surface positions were measured using variable differential transformer sensors. Fuel measurements were obtained from the three fuselage and two

wing tanks. Fuel measurements were used to compute total aircraft weight, center of gravity, and mass moments of inertia. Mass and geometry characteristics of the aircraft are given in Table 1. Sensor positions and the center of gravity (c.g.) location were used to correct the linear accelerometer and flow angle measurements to the c.g. Angular accelerations were not measured. Flight data was collected at 40 Hz.

B. S-2 Subscale Jet Transport Aircraft Description

The S-2 aircraft is a subscale model of a jet transport aircraft A photograph of the aircraft in flight is shown in Fig. 2. The subscale aircraft has a single jet engine mounted in the aft fuselage and retractable tricycle landing gear. Mass and geometry characteristics of the aircraft are given in Table 1. Further information on the S-2 subscale jet aircraft and associated flight test operations can be found in Ref. 17.

Figure 2. **S-2 Subscale Jet Transport Aircraft**

1. Control Surfaces

Control surfaces on the aircraft are conventional elevator, aileron, rudder, and inboard trailing-edge flaps. Definitions of control surface deflections are given below. Trailing edge down is positive deflection for the wing and elevator surfaces, and trailing edge left is positive for the rudder:

$$\delta_e = \frac{1}{2}\left(\delta_{e_{right}} + \delta_{e_{left}}\right) \qquad \delta_a = \frac{1}{2}\left(\delta_{a_{right}} - \delta_{a_{left}}\right) \tag{25}$$

The aircraft can be flown by a safety pilot using direct visual contact and conventional radio control. A research pilot executes flight test maneuvers from inside a mobile control room, using a synthetic vision display drawn from telemetry data and a local terrain database. Inputs from the research pilot and ground-based flight control are used to compute control surface commands which are transmitted by telemetry to the aircraft.

2. Instrumentation and Data Acquisition

The S-2 aircraft was equipped with a micro-INS, which provided 3-axis linear accelerometer measurements, angular rate measurements, estimated attitude angles, and GPS velocity and position. Air data probes on each wingtip (visible in Fig. 2) measured angle of attack, sideslip angle, static pressure, and dynamic pressure. Measurements from static pressure sensors and ambient temperature sensors were used to compute air density and altitude. Engine speed in rpm was measured and used as input to an engine model to compute thrust. The engine model was identified from ground test data, with adjustments for ram drag identified from flight data[18]. Potentiometers on the rotation axes of all control surfaces measured control surface deflections. Mass properties were computed based on measured fuel flow, pre-flight weight and balance, and careful inertia measurements of the aircraft on the ground. The pilot stick and rudder pedal commands and throttle position were also measured and recorded. Flight data was collected at 50 Hz.

IV. Results

A. Data Information Requirements for Real-Time Dynamic Modeling

In this section, results will be presented from investigations concerning data information content necessary for accurate real-time modeling.

Figure 3 shows a relationship between signal-to-noise ratio of aircraft measured responses to the mean error in real-time parameter estimates computed using the FTR method described earlier. Data for this analysis was generated with a linear simulation of the modified F-15B lateral dynamics at a flight condition of Mach 0.75, trim angle of attack 2 deg, and 20,000 ft altitude. Optimized multi-sine inputs were applied simultaneously to the lateral control surfaces, as shown in Fig. 4. Repeated simulated data runs with different output signal-to-noise ratios were generated by uniformly reducing the amplitudes of the inputs shown in Fig. 4, generating new simulated outputs, then adding a single realization of noise sequences extracted from flight data to the simulated outputs. This caused the output signal-to-noise ratios to vary in a uniformly decreasing fashion. For each data run, the FTR method was applied, with no prior information, to produce real-time parameter estimates. Final parameter estimates and

standard errors from each 18 sec run were used to generate the data points for the solid line in Fig. 3. Because the problem involves multiple parameters and multiple outputs, average values of the parameter estimate accuracies and output signal-to-noise ratios were used to make the simple summary plot shown in Fig. 3. Based on the solid line in Fig. 3, signal-to-noise ratios of the measured aircraft responses should preferably be 10 or more, and not less than about 3, for reasonable accuracy of the real-time parameter estimates. This finding is important in designing excitation inputs, and also suggests that lower levels of excitation could be used to obtain accurate real-time dynamic modeling if noise levels were decreased. It is of interest to obtain good real-time parameter estimation results with the lowest possible signal-to-noise ratio on the measured outputs, so that the aircraft and pilot are disturbed as little as possible by any excitation applied to the control surfaces. For output signal-to-noise ratio equal to 10, the input amplitudes were 0.24 deg, and the mean parameter estimate error was 2.7 percent. This choice of input amplitudes produced excellent parameter estimate accuracy, while keeping the root-mean-square value of the lateral acceleration a_y below 0.02 g. A typical value for root-mean-square lateral acceleration in moderate turbulence is 0.05 g.

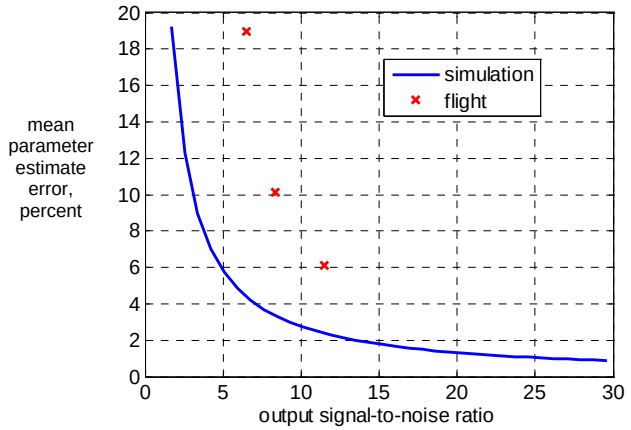

Figure 3. **Dependence of mean real-time parameter estimation error on output signal-to-noise ratio**

Similar optimized multi-sine inputs shown in Fig. 5 were applied to the modified F-15B aircraft in flight at the same flight condition, Mach 0.75, 2 deg trim angle of attack, and 20,000 ft altitude. The aircraft is longitudinally unstable at this flight condition, so feedback control was operating when the control surface excitations were applied by summation with actuator commands from the control system. As shown in Fig. 5, all longitudinal and lateral control surfaces were moved simultaneously. The dashed lines show the optimized multi-sine input design, where the inputs are mutually orthogonal in both the time and frequency domains. The solid lines show the actual control surface measurements in flight, which are distorted from the optimal waveforms. The highest pair-wise correlation for control surface deflections is between stabilator δ_s and canard δ_c, because of the high-gain feedback necessary to compensate for the longitudinal instability at this flight condition. Nevertheless, the control surface deflections were largely uncorrelated, as shown by the pair-wise correlation coefficients listed in Table 2. These correlation levels are well below the 0.9 correlation level typically used as an upper limit for allowable correlation of explanatory variables[6]. Although the relatively high-gain feedback control ruined the input orthogonality, the data still exhibited very low correlations among the control surface deflections, which is desirable for accurate dynamic modeling[6].

Using optimized multi-sine inputs, the effect of input amplitude was investigated by repeating maneuvers with varying input amplitudes. Figure 6 shows the variation in amplitudes for lateral control surface deflections in flight. Selected real-time parameter estimates are shown in Fig. 7. The markers (x, o, +) indicate real-time parameter estimates, while the lines only connect these markers to more clearly show the evolution of the parameter estimates. Real-time modeling was done using the FTR method with no prior information, frequency vector $\boldsymbol{f} = [0.10 \quad 0.12 \quad \ldots \quad 2.00]$ Hz, recursive Fourier transform run at a data rate of 40 Hz, and real-time parameter estimation calculations were done at 2 Hz. Selections for the frequency vector and update rates were not critical to the results produced – similar results could be obtained for a fairly wide-range of choices of these quantities. The results shown in Fig. 7 are typical of all of the real-time parameter estimation results. The excitation amplitudes made little difference in either the speed of convergence or the final parameter estimates. In general, control derivative estimates (e.g., $\hat{C}_{l_{\delta_{ds}}}$) were the fastest to converge and usually the most accurate, followed by static stability derivative estimates (e.g., $\hat{C}_{n_\beta}$) and damping parameter estimates (e.g., $\hat{C}_{l_r}$). Roughly 8 sec of excitation was required for all model parameters to converge, with no prior information. Standard errors are not shown in Fig. 7, to reduce clutter on the plots.

The mean signal-to-noise ratios for the measured lateral aircraft responses in flight to low, medium, and high amplitude inputs were 6.5, 8.4, and 11.5, respectively, with mean parameter estimate errors 19.0, 10.1, and 6.1 percent, respectively. These results are shown by the x markers in Fig. 3, and exhibit the same character as the simulation results shown in Fig. 3, but with higher mean parameter errors. This is expected, because flight data has noise components from structural responses, nonlinearities, and model structure errors that are not present in the linear simulation. This results in higher mean parameter errors for flight data analysis and modeling. The root-mean-square values of the lateral acceleration a_y for low, medium, and high amplitude inputs were 0.012 g, 0.024 g, and 0.045 g, respectively, compared to 0.05 g, which is typical for moderate turbulence.

Variation in the frequency content of the excitation inputs was studied by applying two different optimized excitation input designs in flight, one for a short (6 sec) time length and consequently more sparse frequency content, and one with a longer (15 sec) time length and richer frequency content. A comparison of the frequency content for the two optimized input designs is shown in Fig. 8 for the longitudinal controls only. The spectra comparison for lateral controls was similar. Both optimized input designs were flown on the modified F-15B aircraft, at the same flight condition as before. Typical real-time parameter estimation results are shown in Fig. 9, with 95 percent confidence intervals, based on estimated parameter standard errors, shown by the vertical bars through each estimate. In general, the more sparse frequency content led to slightly poorer convergence and accuracy, except for control derivatives like $\hat{C}_{n_{\delta_r}}$. Figure 9 shows that a more effective approach for short excitation times is to truncate a maneuver designed for a longer time length, because the longer maneuver has a wider variety of frequencies, more closely spaced along the frequency axis, cf. Fig. 8.

Figure 10 shows a comparison of selected real-time parameter estimates based on flight data from the modified F-15B aircraft at the same flight condition. Optimized multi-sine excitation was done first by moving only the longitudinal control surfaces $(\delta_s$ and $\delta_c)$ simultaneously, then again moving all longitudinal and lateral control surfaces $(\delta_s, \delta_c, \delta_a, \delta_r, \delta_{dc},$ and $\delta_{ds})$ simultaneously. The results in Fig. 10 show that there was essentially no difference in the real-time parameter estimation behavior for these cases, indicating that the multiple input design was effective, the equation-error parameter estimation worked as expected on each equation individually, and finally that there was negligible aerodynamic coupling for the maneuvers resulting from these optimized excitation inputs. Similar results were found when comparing lateral excitation alone to combined longitudinal and lateral excitation. Real-time parameter estimate behavior for other model parameters was similar to what is shown in Fig. 10 for the three selected longitudinal parameters.

The results in Fig. 10 indicate that combined longitudinal and lateral maneuvers with all control surfaces moving at once should be used for maximum efficiency in real-time dynamic modeling. This approach can provide a full set of stability and control modeling results in a single relatively short maneuver. Finally, Fig. 10 shows that the FTR method has no trouble identifying dynamic model parameters when the aircraft is statically unstable longitudinally $(C_{m_\alpha} > 0)$, as in this case.

B. Prior Information

The real-time dynamic modeling results shown in Figs. 7, 9, and 10 were generated with the FTR algorithm assuming no priori information. If instead the FTR algorithm is provided some information on the values of the model parameters, in terms of parameter estimates and associated covariance matrix from a prior analysis, the convergence behavior of the real-time parameter estimates from the FTR method changes. Figure 11 shows real-time parameter estimate histories for a combined longitudinal and lateral maneuver using medium-amplitude optimized multi-sine excitation and no prior information, along with real-time parameter estimate histories using the same data, but with prior information from parameter estimates and associated covariance matrix at the end of a low-amplitude combined maneuver. Real-time estimate variations are greatly reduced with the addition of prior information, particularly at the beginning of the maneuver. However, this regularization also results in something like a weighted average for the final parameter estimate, which is different from what would be computed with no prior information, as can be seen in the top plot of Fig. 11 for $\hat{C}_{m_q}$. The extent of this effect depends on the values and accuracy of the parameter estimates provided as prior information.

C. Model Validity

The quality of the estimated parameter error bounds can be judged by how well the error bounds characterize the difference between the associated real-time parameter estimate and the final converged parameter estimate. The computed error bounds from the FTR method accurately characterized these differences, which is consistent with similar findings in previous work[6,13]. Although such a measure is easy to compute post-flight (when the converged values are known), metrics that can be computed in real time must be devised. Adequacy of local real-time dynamic models can be assessed using short-term prediction tests or tests involving the size of the estimated parameter standard errors. Various metrics have been proposed, but research continues toward devising a generally-applicable metric for real-time model validation.

Table 3 gives parameter estimates and standard errors from the FTR method at the end of a high amplitude lateral maneuver (for the lateral parameters) and a medium amplitude longitudinal maneuver (for the longitudinal parameters), with no prior information. Separate maneuvers with different amplitudes were chosen to more closely match the amplitudes of doublet maneuvers used for prediction testing. Model parameters given in Table 3 were used with control surface deflections from pilot doublet maneuvers to check prediction capability of the identified models. Bias terms for the aerodynamic models were estimated in the time domain[6], because the frequency-domain modeling excludes the biases.

Figure 12 shows model predictions using flight data from a longitudinal pilot doublet maneuver (on the left) and a lateral/directional pilot doublet maneuver (on the right). For these pilot doublet maneuvers, the control surface deflections were highly correlated with one other and with aircraft responses. Consequently, pilot doublet maneuvers could only be used for prediction cases, and not for model identification. In Fig. 12, the responses predicted with models identified from multi-sine inputs match the flight data within the noise level of the measured responses of the aircraft for most of each maneuver. The prediction capability shown in Fig. 12 is excellent for these doublet maneuvers, which have very different input forms than the multi-sine inputs used in the identification maneuvers. This gives high confidence in the validity of the identified models.

D. Real-Time Dynamic Modeling in Operational Flight

All of the flight testing for dynamic modeling on the modified F-15B aircraft was at a single flight condition, using various optimized excitation inputs. To investigate the performance of the real-time dynamic modeling method in operational flight with low data information content, flight data from the S-2 subscale jet transport aircraft in normal approach (i.e., without specific excitation inputs) was used. Figure 13 shows real-time parameter estimation results for the S-2 aircraft during approach in landing configuration (full flaps, landing gear down). The real-time parameter estimates shown in Fig. 13 were obtained with no prior information.

The real-time dynamic modeling results in this case are of similar quality to the results obtained with optimized multi-sine excitation inputs. Part of the reason for this is that the S-2 aircraft must be actively controlled by the pilot during approach to landing, and there is no feedback control system operating. However, these results show encouraging success in estimating real-time dynamic model parameters without specific control surface excitation. Further flight research is planned for the S-2 aircraft, which has been equipped with the capability to apply arbitrary excitations to any or all control surfaces. This capability will be used to investigate lower limits on signal-to-noise ratios for real-time dynamic modeling in changing flight conditions and for real-time dynamic modeling near stall and departure.

Real-time dynamic modeling was also applied in S-2 flight testing during 3-axis pilot doublet maneuvers (pitch, yaw, and roll doublets, in sequence), with results displayed inside the mobile operations station (MOS)[18] in real time. Figure 14 shows the real-time display for selected parameter estimates during a 3-axis pilot doublet maneuver at 80 knots and 800 ft altitude. The dashed lines (added post-flight) indicate values of the parameter estimates obtained using a time-domain output-error method that employs an iterative nonlinear optimizer in post-flight batch mode[6]. It is evident that after only a few seconds of data, the real-time dynamic modeling algorithm (operating with no prior information) computed very accurate stability and control derivative estimates. Note that each stability or control derivative is inaccurate until the relevant measured quantity shows some significant variation (i.e., data information content), after which the associated derivative estimate converges quickly. Finally, the 95 percent confidence intervals for the parameter estimates, indicated by the vertical bars through each parameter estimate marker, properly characterize the accuracy of the real-time parameter estimates.

V. Concluding Remarks

Simulated data and flight test results were used to investigate data information requirements for accurate real-time dynamic modeling. This technology provides the capability to identify local dynamic models in real time from noisy data records. With proper data information management, the approach could be applied to changing flight conditions that occur throughout a flight, and/or could identify local dynamics for cases of failure or damage that can be characterized by model parameter changes.

A real-time dynamic modeling algorithm was described in detail. The algorithm uses equation-error in the frequency domain, and a recursive Fourier transform. Modifications necessary to incorporate information from a previous analysis into the least squares formulation, or to implement data forgetting in the frequency domain, were developed and explained.

Results from flight investigations on a modified F-15B aircraft showed that optimized multi-sine inputs provided excellent data information content for real-time dynamic modeling, even with a relatively high-gain feedback control system operating. Mean signal-to-noise ratio of aircraft flight responses was inversely correlated with mean real-time parameter estimation error, based on analysis of both simulation data and flight data from the modified F-15B aircraft. This suggests that smaller excitations can be used as measurement noise levels get smaller, making the required excitations less noticeable to the pilot. Refinements to the optimized excitation input designs were identified based on flight results. Combined longitudinal and lateral optimal excitations were found to efficiently provide data information content for real-time dynamic modeling in all axes simultaneously. Incorporating information about the dynamic model parameters from a prior analysis into the real-time modeling algorithm was shown to effectively reduce variability in real-time parameter estimates, particularly at the start of a maneuver. However, using this approach makes the parameter estimator respond more slowly to changing aircraft stability and control characteristics. Real-time estimates of parameter errors computed from flight data were found to properly characterize the accuracy of the real-time parameter estimates. Dynamic models identified in real time showed excellent prediction capability for maneuvers with dissimilar input forms. Finally, flight data from a subscale jet transport aircraft was used to show that the real-time dynamic modeling can also work well for 3-axis pilot doublet maneuvers, as well as ordinary flight operations maneuvers, such as approach to landing.

Future work could focus on the data management problem, i.e., how much data information to forget and when, as well as determining when control surface excitations should be applied. Other extensions include real-time modeling for changing flight conditions and different aircraft configurations, as well as real-time modeling for aircraft degradations such as aging, damage, and failures.

Uses for local real-time dynamic modeling results include improving stability and control flight testing efficiency, and prediction of dynamic behavior and departure. Identified local linear models can be also used in real time to track eigenvalues and eigenvectors of the dynamic system. This information can be used in bifurcation analysis for nonlinear flight regimes.

Acknowledgments

The efforts of the F-15 flight test team at NASA Dryden and the AirSTAR flight test team at NASA Langley, in building and testing the aircraft and associated systems, carefully calibrating the instrumentation, and carrying out the flight operations to collect the high-quality flight data used in this study, are gratefully acknowledged. Research in real-time dynamic modeling is funded by the NASA Aviation Safety Program, Integrated Resilient Aircraft Control (IRAC) project.

References

[1]Bauer, J.E. and Andrisani, D. "Estimating Short-Period Dynamics Using an Extended Kalman Filter," NASA TM 101722, June 1990.

[2]Garcia-Velo, J. and Walker, B.K. "Aerodynamic Parameter Estimation for High-Performance Aircraft Using Extended Kalman Filtering," *Journal of Guidance, Control, and Dynamics*, Vol. 20, No. 6, November-December 1997, pp. 1257-1259.

[3]Ward, D.G., Monaco, J.F., and Bodson, M. "Development and Flight Testing of a Parameter Identification Algorithm for Reconfigurable Control," *Journal of Guidance, Control, and Dynamics*, Vol. 21, No. 6, November-December 1998, pp. 948-956.

[4]Morelli, E.A. "Real-Time Parameter Estimation in the Frequency Domain," *Journal of Guidance, Control, and Dynamics*, Vol. 23, No. 5, September-October 2000, pp. 812-818.

[5]Valasek, J. and Chen, W. "Observer/Kalman Filter Identification for Online System Identification of Aircraft," *Journal of Guidance, Control, and Dynamics*, Vol. 26, No. 2, March-April 2003, pp. 347-353

[6]Klein, V. and Morelli, E.A., *Aircraft System Identification – Theory and Practice*, AIAA Education Series, AIAA, Reston, VA, 2006.

[7]Basappa, K. and Jategaonkar, R. "Evaluation of Recursive Methods for Aircraft Parameter Estimation," AIAA-2004-5063, *Atmospheric Flight Mechanics Conference and Exhibit*, Providence, RI, August 2004.

[8]Song, Y., Campa, G., Napolitano, M.R., Seanor, B., and Perhinschi, M.G. "Online Parameter Estimation Techniques Comparison Within a Fault Tolerant Flight Control System," *Journal of Guidance, Control, and Dynamics*, Vol. 25, No. 3, May-June 2002, pp. 528-537.

[9]Smith, M.S., Moes, T.R., and Morelli, E.A. "Real-Time Stability and Control Derivative Extraction From F-15 Flight Data," AIAA 2003-5701, *AIAA Atmospheric Flight Mechanics Conference*, Austin TX, August 2003.

[10]Moes, T.R., Smith, M.S., and Morelli, E.A. "Flight Investigation of Prescribed Simultaneous Independent Surface Excitations for Real-Time Parameter Identification," AIAA 2003-5702, *AIAA Atmospheric Flight Mechanics Conference*, Austin TX, August 2003.

[11]Morelli, E.A. "Multiple Input Design for Real-Time Parameter Estimation in the Frequency Domain," Paper REG-360, *13th IFAC Symposium on System Identification*, Rotterdam, The Netherlands, August 2003.

[12]Morelli, E.A. "High Accuracy Evaluation of the Finite Fourier Transform using Sampled Data," NASA TM 110340, June 1997.

[13]Morelli, E.A., "Practical Aspects of the Equation-Error Method for Aircraft Parameter Estimation," AIAA-2006-6144, *AIAA Atmospheric Flight Mechanics Conference*, Keystone, CO, August 2006.

[14]Press, W.H., S.A. Teukolsky, W.T. Vettering, and B.R. Flannery *Numerical Recipes in FORTRAN: The Art of Scientific Computing*, 2nd Ed., Cambridge University Press, New York, NY, 1992, Chapter 10.

[15]Morelli, E.A. "Flight Test Experiment Design for Characterizing Stability and Control of Hypersonic Vehicles," AIAA-2008-1682, *U.S. Air Force T&E Days*, Los Angeles, CA, February 2008.

[16]Doane, P., R. Bursey, and G. Schkolnik (1994) "F-15 ACTIVE: A Flexible Propulsion Integration Testbed," AIAA 94-3361.

[17]Jordan, Thomas L., Foster, John V., Bailey, Roger M., and Belcastro, Christine M.; "AirSTAR: A UAV Platform for Flight Dynamics and Control System Testing", AIAA-2006-3307, *25th AIAA Aerodynamic Measurement Technology and Ground Testing Conference*, San Francisco, CA, June 2006.

[18]Cunningham, K., Foster, J.V., Morelli, E.A., and Murch, A.M., "Practical Application of a Subscale Transport Aircraft for Flight Research in Control Upset and Failure Conditions," AIAA-2008-6200, *AIAA Atmospheric Flight Mechanics Conference*, Honolulu, HI, August 2008.

Table 1. Geometry and mass properties

	Modified F-15B	S-2
length $\bar{c}$, ft	15.94	0.908
wing span b , ft	42.70	7.083
wing area S , ft^2	608.0	7.046
x_{ref} , in	557.2	42.628
y_{ref} , in	0.000	0.000
z_{ref} , in	116.3	0.000
x_{cg} , in	560.40	42.728
y_{cg} , in	0.14	0.000
z_{cg} , in	117.41	0.519
m , slugs	1234	1.502
I_x , slugs-ft^2	24,830	1.077
I_y , slugs-ft^2	196,225	4.163
I_z , slugs-ft^2	216,155	5.016
I_{xz} , slugs-ft^2	–5329	0.416

Table 2. Pair-wise correlation matrix for control surface deflections

	δ_s	δ_c	δ_a	δ_r	δ_{dc}	δ_{ds}
δ_s	1	–0.293	–0.085	–0.026	0.126	0.016
δ_c		1	–0.120	–0.065	–0.043	–0.149
δ_a			1	0.083	0.011	–0.010
δ_r				1	0.177	–0.029
δ_{dc}					1	–0.059
δ_{ds}						1

Table 3. Converged real-time parameter estimates for the modified F-15B from combined longitudinal/lateral optimized multi-sine flight test maneuvers

$V_o = 793$ ft/sec, $h_o = 20{,}000$ ft, $\alpha_o = \theta_o = 2$ deg

Parameter θ	Estimate $\hat{\theta}$	Standard Error s
C_{Z_α}	–4.5302	0.0397
C_{Z_q}	–12.6864	0.6370
$C_{Z_{\delta_s}}$	–0.4958	0.0150
$C_{Z_{\delta_c}}$	–0.1816	0.0238
C_{m_α}	0.2339	0.0234
C_{m_q}	–2.9742	0.3746
$C_{m_{\delta_s}}$	–0.5521	0.0088
$C_{m_{\delta_c}}$	0.2544	0.0140
C_{Y_β}	–0.7646	0.0114
C_{Y_r}	1.7568	0.1402
$C_{Y_{\delta_a}}$	0.0264	0.0064
$C_{Y_{\delta_r}}$	0.2068	0.0038
$C_{Y_{\delta_{dc}}}$	–0.0980	0.0057
$C_{Y_{\delta_{ds}}}$	0.1546	0.0068
C_{l_β}	–0.0678	0.0037
C_{l_p}	–0.2009	0.0104
C_{l_r}	0.2383	0.0432
$C_{l_{\delta_a}}$	–0.0625	0.0020
$C_{l_{\delta_r}}$	0.0048	0.0012
$C_{l_{\delta_{dc}}}$	0.0005	0.0018
$C_{l_{\delta_{ds}}}$	–0.0777	0.0024
C_{n_β}	0.0945	0.0041
C_{n_p}	–0.0348	0.0115
C_{n_r}	–0.3154	0.0477
$C_{n_{\delta_a}}$	–0.0092	0.0023
$C_{n_{\delta_r}}$	–0.0805	0.0013
$C_{n_{\delta_{dc}}}$	–0.0518	0.0020
$C_{n_{\delta_{ds}}}$	–0.0474	0.0027

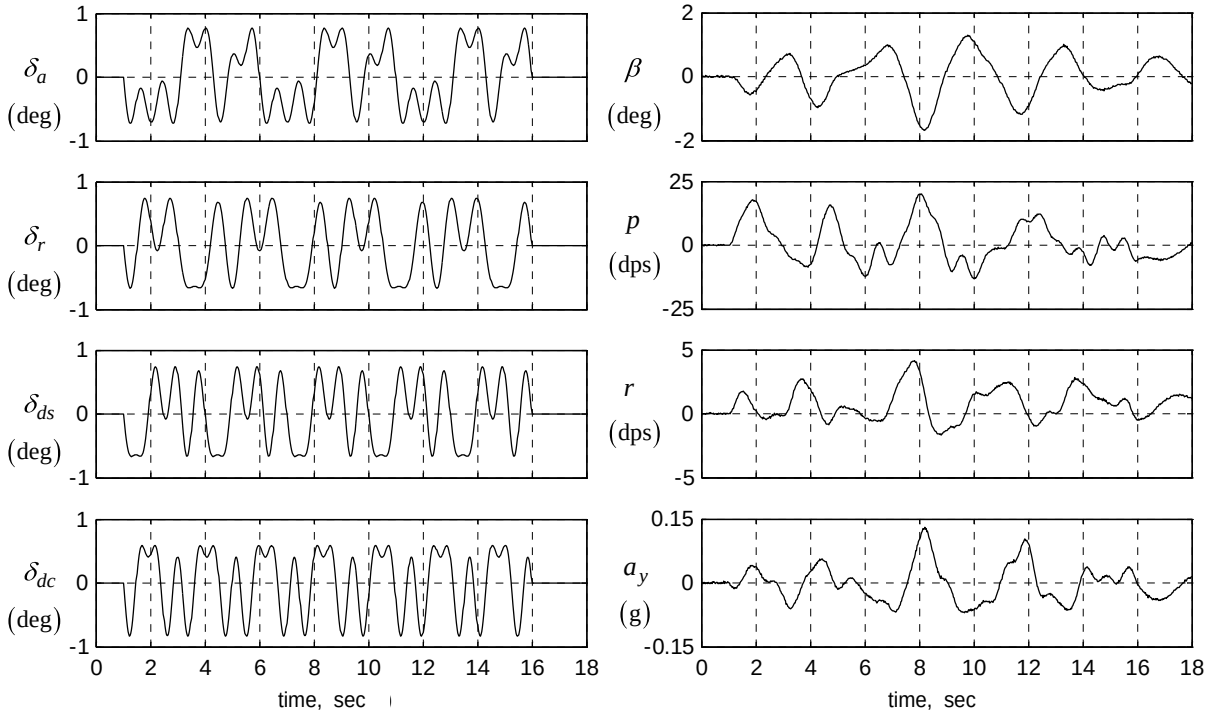

Figure 4. **Simulated data for optimized multi-sine inputs, modified F-15B aircraft**

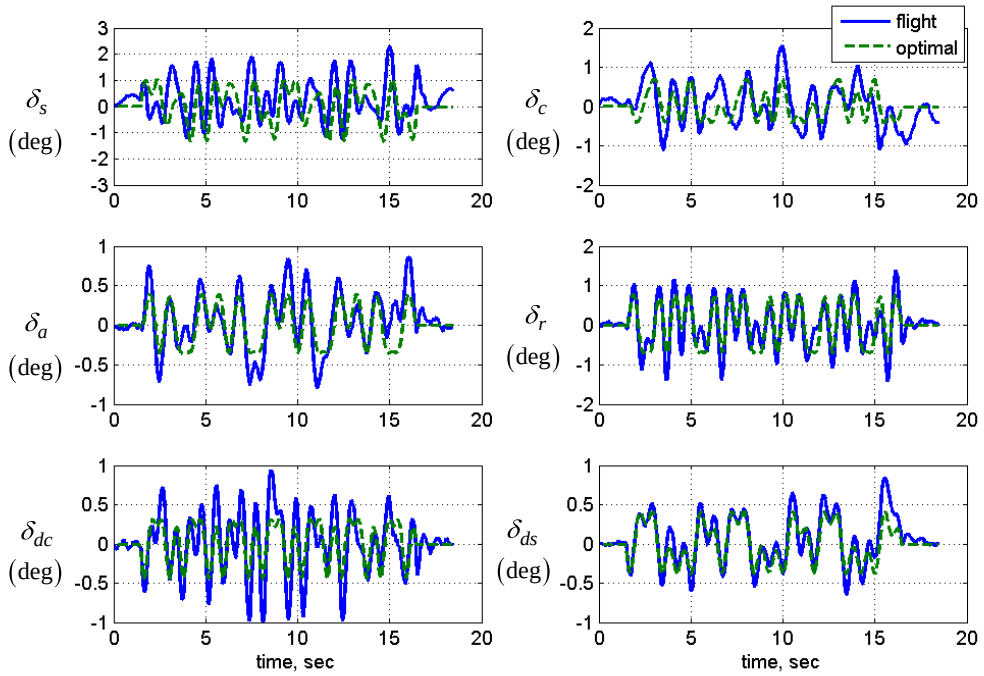

Figure 5. **Optimized multi-sine input distortion, modified F-15B aircraft**

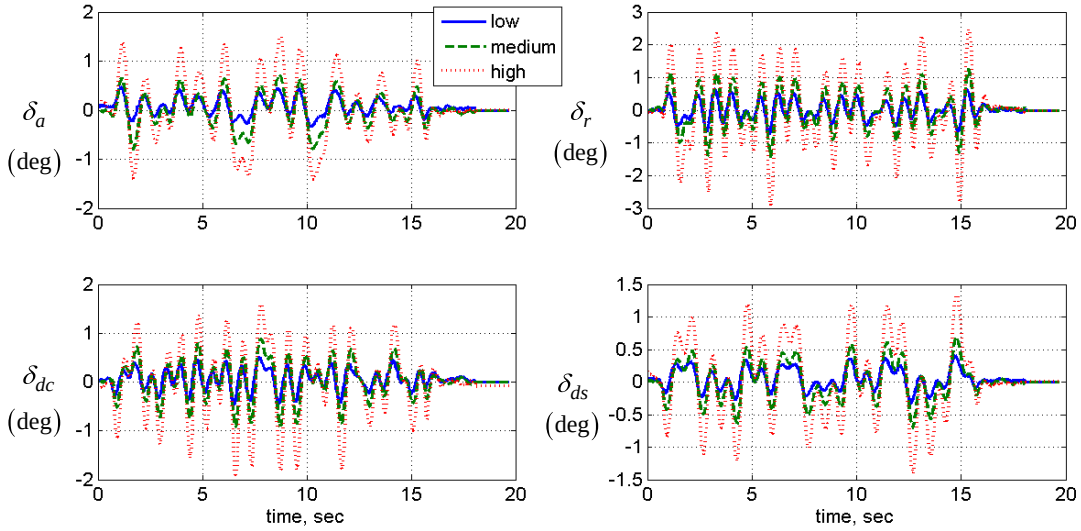

Figure 6. **Input amplitude variation, modified F-15B aircraft**

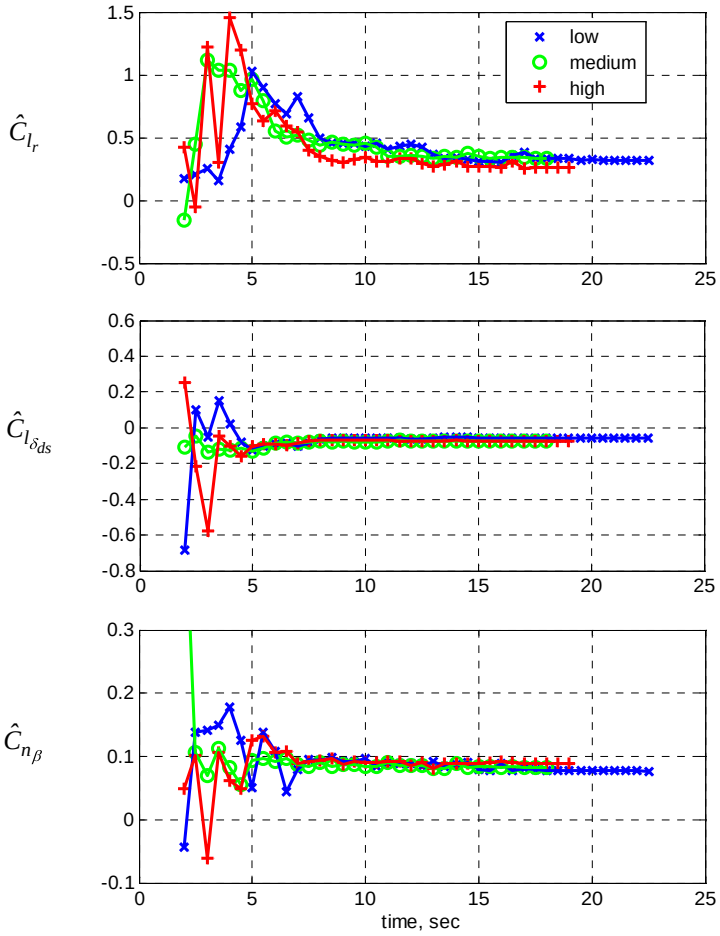

Figure 7. **Real-time parameter estimates for varying input amplitudes, modified F-15B aircraft**

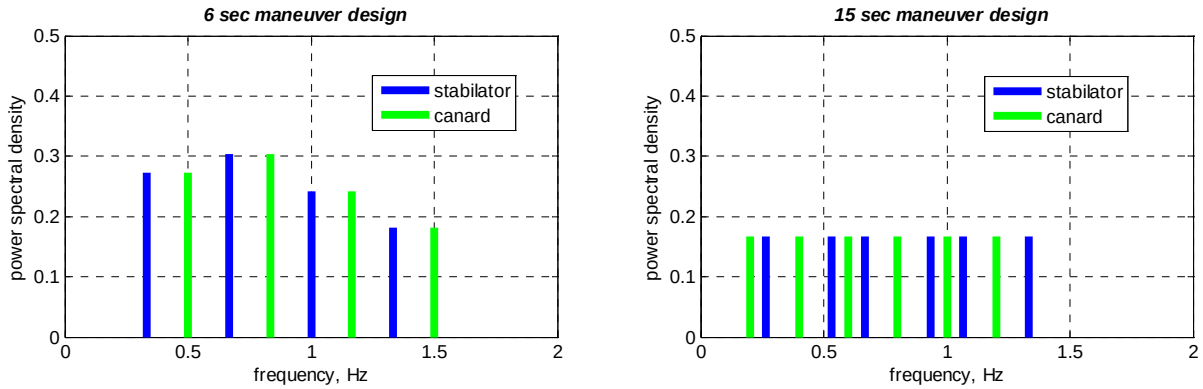

Figure 8. **Excitation input spectra for 6 sec and 15 sec longitudinal controls, modified F-15B aircraft**

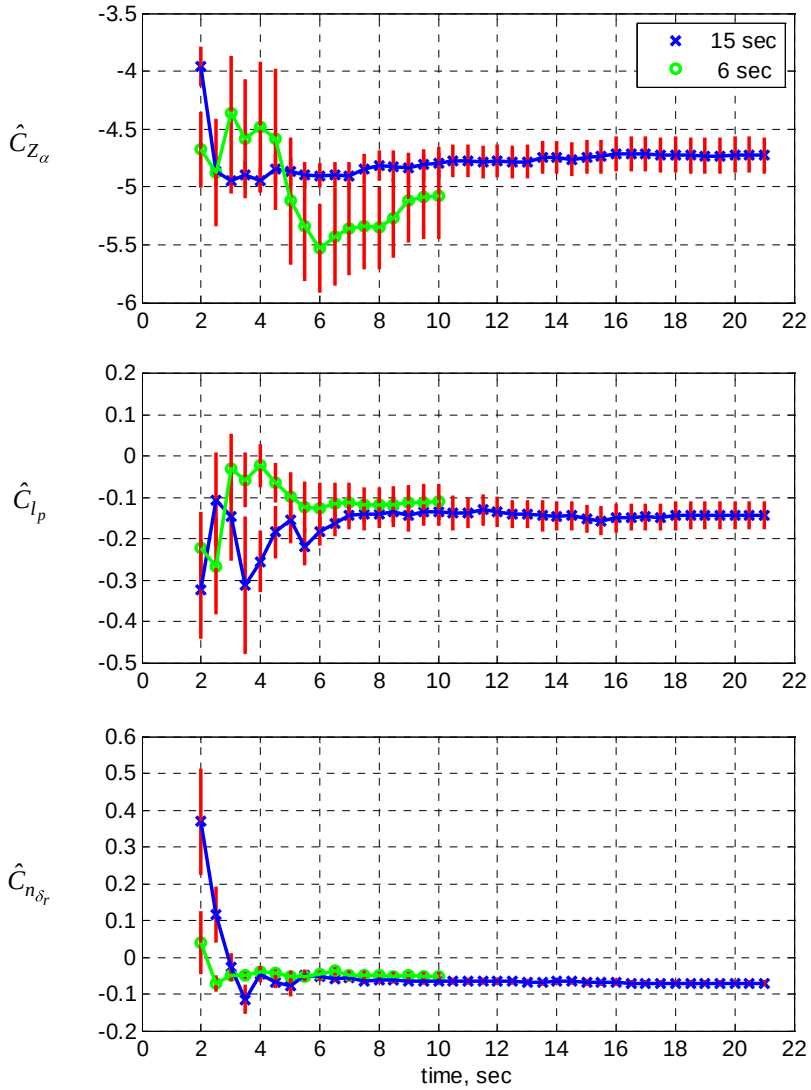

Figure 9. **Real-time parameter estimates for varying frequency content, modified F-15B aircraft**

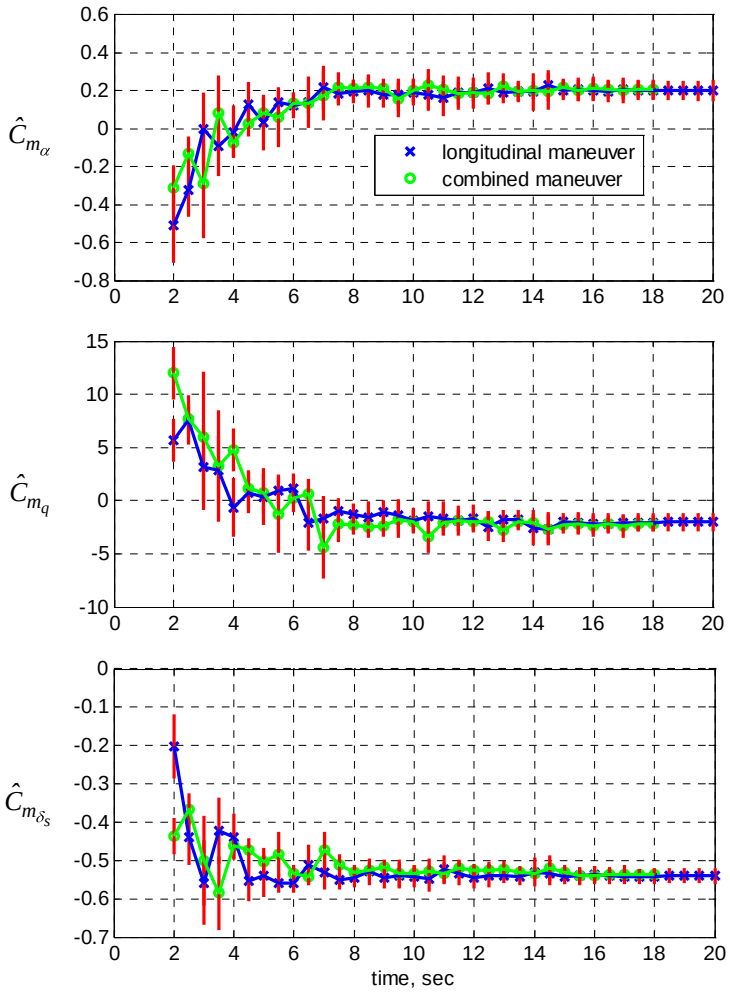

***Figure 10*. Real-time parameter estimates for combined maneuver compared to longitudinal only, modified F-15B aircraft**

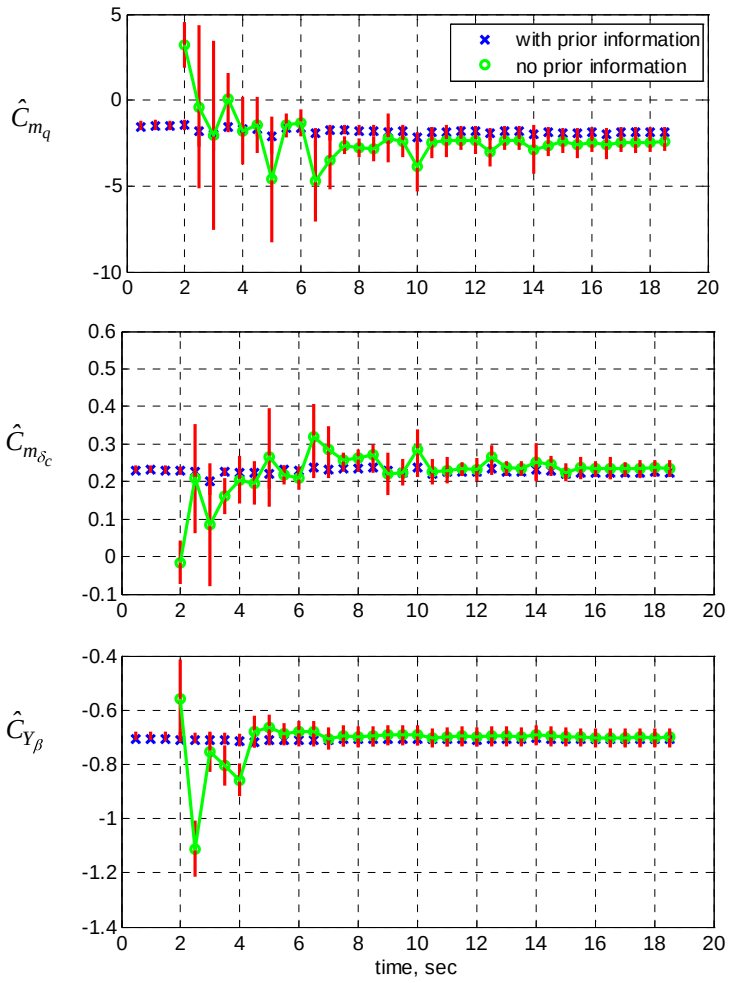

Figure 11. **Real-time parameter estimates with and without prior information, modified F-15B aircraft**

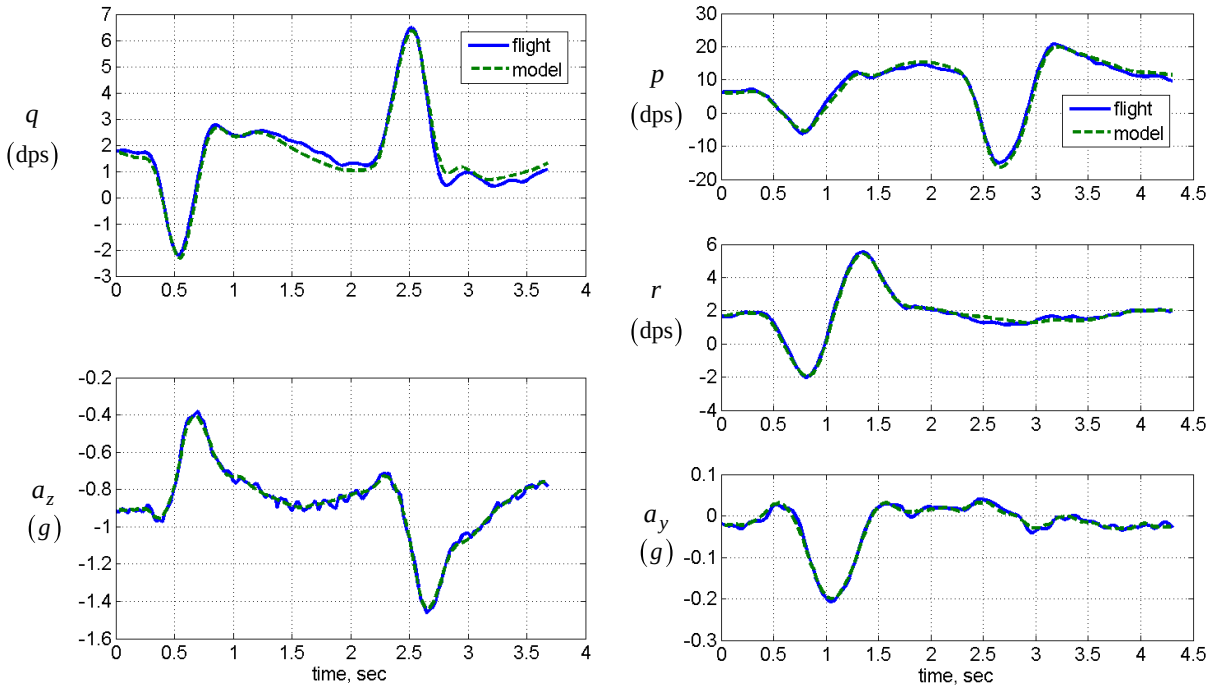

Figure 12. **Prediction cases using real-time parameter estimates, modified F-15B aircraft**

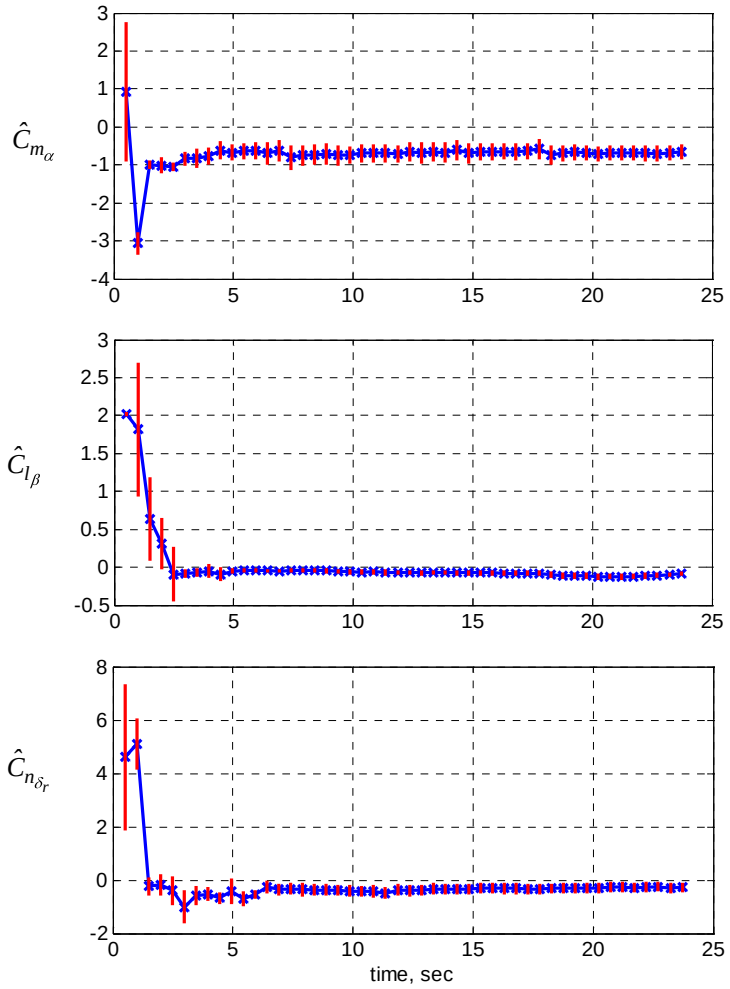

Figure 13. **Real-time parameter estimates during approach in landing configuration, S-2 aircraft**

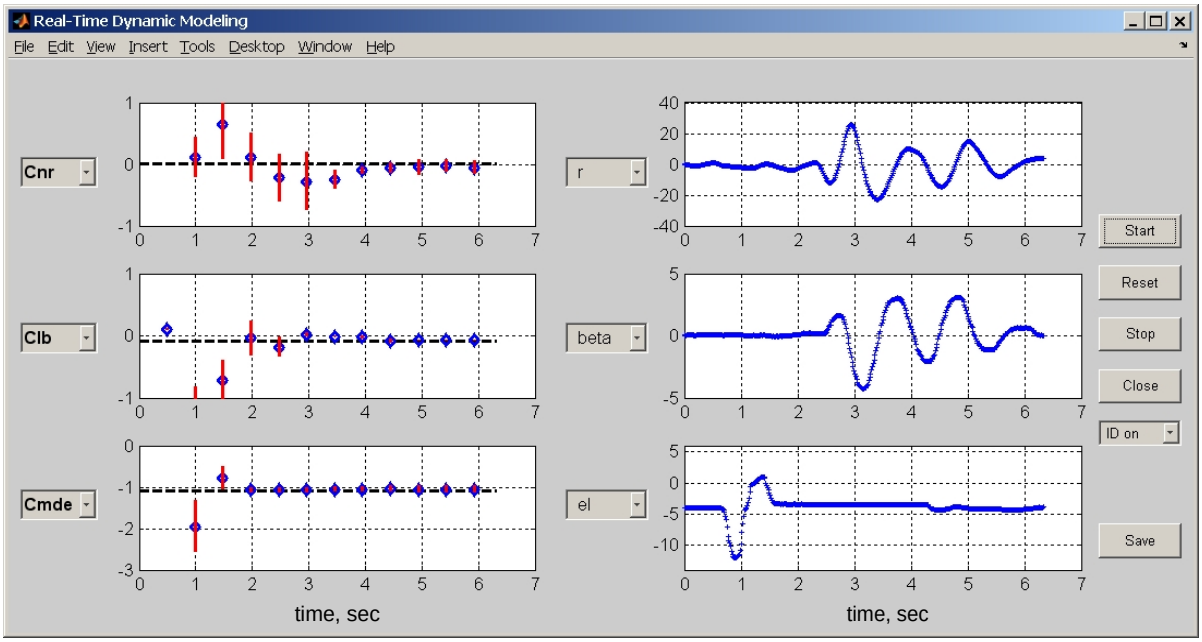

Figure 14. **Real-time parameter estimates for a 3-axis pilot doublet maneuver, S-2 aircraft**